Graefe's Arch Clin Exp Ophthalmol (2007) 245:1773–1780
DOI 10.1007/s00417-007-0610-9

CLINICAL INVESTIGATION

Transcorneal electrical stimulation of retina to treat longstanding retinal artery occlusion

Koichi Inomata · Kei Shinoda · Hisao Ohde · Kazushige Tsunoda · Gen Hanazono · Itaru Kimura · Mitsuko Yuzawa · Kazuo Tsubota · Yozo Miyake

Received: 19 October 2006 / Revised: 12 April 2007 / Accepted: 14 May 2007 / Published online: 26 June 2007

Abstract
Purpose To report the outcome of transcorneal electrical stimulation (TES) of the visual system on long-standing retinal artery occlusion (RAO).
Design Open labeled, case series.
Patients and methods Two patients with central RAO (15 and 33 months respectively) and one with branch RAO (26 months) underwent TES therapy. Subjective and objective ophthalmological evaluations were performed before and after the TES. The ages of the patients were 38, 49, and 63 years. The TES (20 Hz biphasic pulses, 30 minutes, up to 1100 uA) was delivered by a bipolar contact lens electrode once a month for 3 months. Perimetric and/or electrophysiological examinations were performed as outcome measures.
Results The visual acuity improved by more than 0.2 logMAR units in two cases, and the visual fields were improved in all three cases. The multifocal ERGs which had been reduced in the loci corresponding to the ischemic retinal area were improved after the treatment in two cases. Neither ocular nor systemic adverse effects were observed except for transient superficial keratitis.
Conclusions TES of the retina can improve retinal function in eyes with long-standing RAOs.

Keywords Phosphene · Electrical stimulation · Central retinal artery occlusion · Branch retinal artery occlusion

None of the authors have any financial or proprietary interest in any material or methods mentioned. This study was supported by Researches on Sensory and Communicative Disorders from the Ministry of Health, Labor, and Welfare, Japan.

K. Inomata · K. Shinoda (✉) · H. Ohde · K. Tsunoda · G. Hanazono · Y. Miyake
Laboratory of Visual Physiology, National Institute of Sensory Organs, National Hospital Organization, Tokyo Medical Center, 2-5-1 Higashigaoka, Meguro-ku, Tokyo 152-8902, Japan
e-mail: shinodakei@kankakuki.go.jp

I. Kimura
Laboratory of Clinical Epidemioogy, National Institute of Sensory Organs, National Hospital Organization, Tokyo Medical Center, 2-5-1 Higashigaoka, Meguro-ku, Tokyo 152-8902, Japan

K. Inomata · H. Ohde · M. Yuzawa
Department of Ophthalmology, School of Medicine, Nihon University, 1-8-13 Surugadai, Kanda, Chiyoda-ku, Tokyo 101-8309, Japan

K. Shinoda · H. Ohde · I. Kimura · K. Tsubota
Department of Ophthalmology, Keio University School of Medicine, 35 Shinanomachi, Shinjuku-ku, Tokyo 160-8582, Japan

H. Ohde
Kamoshita Eye Clinic, 7-15-14 Roppongi, Minato-ku, Tokyo 106-0032, Japan

Introduction

Retinal artery occlusions (RAOs) usually cause sudden, painless, catastrophic visual loss, and the retinal damage progresses every quickly [1–3]. Therefore, an RAO is a true ophthalmic emergency, and therapy must be started as soon as possible, and at the latest within 24 hours after the onset of the visual loss [1]. Several types of treatment have been described for the acute phase, e.g., ocular massage [4, 5], intravenous injection of urokinase and/or prostaglandin [6], hyperbaric oxygenation [7], and anterior chamber paracentesis

[8, 9]. However, there is not enough evidence to decide which treatment is most effective for an acute central RAO, and some therapy may even be harmful [10]. The rapid initiation of treatment is important, because longstanding RAOs lead to irreversible retinal damage, and no effective treatment exists for the retinal damage.

Recent studies have shown that electrical stimulation of different types of neural tissues has a neuroprotective effect, and the mechanism for this effect has been suggested to be an up-regulation of neurotrophic factors [11, 12]. Although the exact mechanism has yet to be determined, several investigators have shown that electrical stimulation up-regulates neurotrophins in the central and peripheral nervous system [13–15]. To examine the effects of electrical stimulation of the retina, investigators have implanted electrodes epi- or subretinally, and they have reported that electrical stimulation up-regulated neurotrophic factors, resulting in a protective effect on the remaining retinal circuitry [16, 17]. The drawback to this treatment is that surgery is required.

Morimoto et al. [13] reported a much less invasive way to activate the retina called transcorneal electrical stimulation (TES), using a contact-lens electrode. This method has long been known to evoke visual sensations (phosphenes) and cortical potentials that stem from the activation of inner retinal neurons [18–21]. These observations prompted us to examine whether TES of the retina will alter the visual function of patients with longstanding retinal RAO.

Patients and methods

Transcorneal electrical stimulation was used on three cases of longstanding retinal artery occlusion; two cases of central retinal artery occlusion (CRAO) and one with a branch retinal artery occlusion (BRAO; Table 1). The procedures used conformed to the tenets of the Declaration of Helsinki, and an informed consent was obtained from each individual who participated in this study after an explanation of the procedures to be used. This prospective interventional case study was approved by the Institutional Review Board of Keio University Hospital.

Biphasic pulses at a frequency of 20 Hz and up to 1100 μA, which elicited both peripheral and central phosphenes, were applied to the affected eye through a bipolar contact-lens electrode (Fig. 1). This stimulus protocol was chosen according to the previous TES study by Fujikado et al. [22]. The bipolar contact-lens electrode (Mayo Corporation, Inazawa, Japan) was placed on the cornea after the cornea was anesthetized with 0.4% oxybuprocaine hydrochloride. The electric current pulses were delivered by a stimulator (BPG-1, BAK Electronics, Inc., Mount Airy, MD, USA) and a stimulus isolation unit (BSI-2, BAK Electronics, Inc.) via circular concentric gold electrodes embedded in the

Table 1 Patients' demographics in the study

Case no.	Age	Gender	Disease	Visualfield deficit pattern	Interval between the onset and the TES therapy (months)	Current of TES which elicited peripheral phosphene (uA)	Current of TES which elicited central phosphenc (uA)	Visual acuity		Electrophysiological testings (ERGs) examined	
								prc treatment	post treatment	pre treatment	post treatment
1	63	M	CRAO	Peripheral island remained	33	600–900	(–)*	0.09	0.15	Bright flash, flicker	Scotopic, bright flash, photopic, flicker
2	49	M	CRAO	Central scotoma	15	800–900	1000–1100	0.06	0.15	Scotopic, bright flash, photopic, flicker, mERG	Scotopic, bright flash, photopic, flicker, mERG
3	38	F	BRAO	Inferonasal deficit	26	200–250	500–600	1.2	1.2	Scotopic, bright flash, photopic, flicker, mERG	Scotopic, bright flash, photopic, flicker, mERG

M: male, F: female, CRAO: central retinal artery occlusion, BRAO: branch retinal artery occlusion
TES transcorneal electrical retinal stimulation, ERG: electroretinogram
*:The visual field in Case 1 consisted of only peripheral regions and the phosphene in the central visual field could not be obtained.

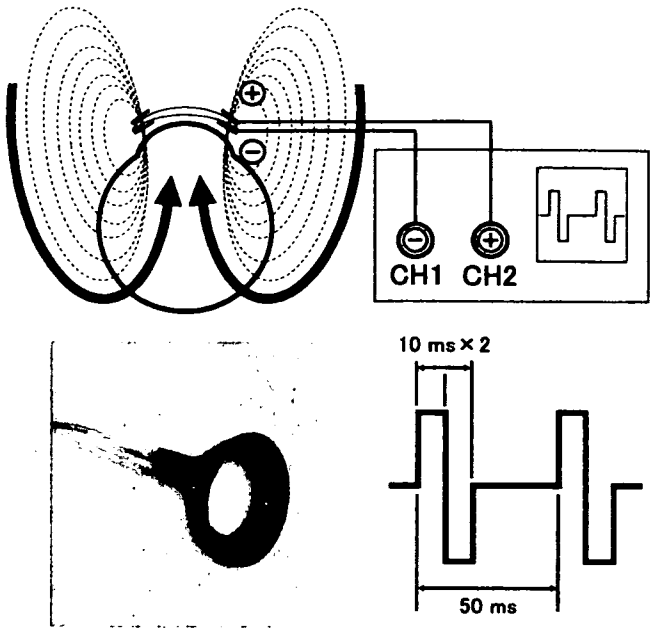

Fig. 1 Bipolar contact lens electrode and pattern of electrical currents. *Top:* Schematic diagram of the pathways of the electrical retinal stimulation therapy. A circular electrical electrode [OE] is attached to the outer surface of the contact lens and makes contact with the palpebral conjunctiva, and another circular electrode [IE] is attached on the inner surface of the contact lens and makes contact with the bulbar conjunctiva. *Dotted lines* and *thick arrows* show the predicted pathway for the electrical current flowing through the retina in both directions. *Bottom left:* Photograph of bipolar contact-lens electrode used to deliver the electrical currents for transcorneal electrical stimulation of the retina. *Bottom right:* The waveform of the current

contact lens (Fig. 1). Hyaluronic acid (3%) and 4% chondroitin sulfate (Viscot, Alcon Japan, Tokyo, Japan) were applied to the inner surface of the contact lens. Initially, the threshold current to elicit phosphenes, which were perceived in the peripheral and central visual fields, was determined by increasing the currents from 0 to 1100 μA. Then the threshold current evoking these phosphenes was applied for 30 minutes at each session, and this stimulation was performed once a month for up to 3 months.

To assess the changes induced, slit-lamp examinations, ophthalmoscopy, Goldmann visual fields, and electrophysiological recordings were made before and 1 month after the third treatment. In addition, the best-corrected visual acuity was determined before and after the TES.

Full-field electroretinograms (ERGs) were recorded in conformity with the ISCEV standards (http://www.iscev.org/standards/index.html). A bipolar contact-lens electrode (Mayo Corporation, Kyoto, Japan) was used to record the ERGs, and the fellow eye was occluded. The ground electrode was attached to the earlobe.

Scotopic, bright-flash, photopic ERGs and flicker ERGs were recorded before and after the treatments in Cases 2 and 3. In Case 1, the bright-flash and flicker ERGs were recorded before the treatments, and the entire series of ERGs were recorded after the treatment (Table 1, Figs. 2, 3 and 4). At examination, each recording was repeated twice or three times to check the reproducibility, and one of the representative recordings was placed in the patient's record. Therefore, the statistical evaluation was not possible for the full-field ERG data.

Multifocal ERGs (mfERGs) were recorded with the VERIS system (Tomey, Nagoya, Japan) using the same bipolar contact-lens electrode. The central 50 degrees of ocular fundus were stimulated by an array of 61 hexagonal stimuli that were displayed on a monochromatic monitor (MD-B1700, Chuomusen Co., Ltd, Tokyo, Japan). The luminance of each hexagon was alternated between black and white according to a pseudorandom binary m-sequence at a rate of 75 Hz. An X-shaped fixation target was displayed at the center of the monitor, and the fixation was carefully monitored during the recordings. The best refractive correction for the target distance was worn during the recordings. The total recording time was 8 minutes, and the recordings were divided into 16 approximately equal segments with rest periods. The signals were amplified 10^5 times, and the bandpass filters were set at 10 and 300 Hz (Model 12 Neurodata Acquisition System; Grass, West Warwick, RI, USA).

The data were analyzed using a VERIS Science 4.1.1 analysis program (Electro Diagnostic Imaging, Redwood City, CA, USA). The averaged local responses from the area corresponding to the central scotoma in Case 2 (Fig. 3), which were expected to be affected by the retinal artery occlusion (area 1, comprising of rings 1 and 2, n=6) were obtained using a multi-input analysis technique. Area 2 (comprised of rings 3, 4, and 5, n=55) was defined as the peripheral area surrounding the central scotoma in Case 2 (Fig. 3).

In Case 3, the averaged local responses (n=16) from the inferior field corresponding to the visual field deficit (area 2 in Fig. 4) were compared to those from a symmetrical area in the superior field (area 1; Fig. 4). The difference between the first negative component and the following positive component (the N1-P1 amplitude), and the latency of the first positive component (the P1 latency) were used for evaluation. The artifact removal and the special averaging procedures were not used.

The mfERGs were measured in Cases 2 and 3 before and after the treatments, but in Case 1 the mfERG was not recorded because the patient's visual field consisted of only peripheral regions, and good fixation could not be obtained (Table 1).

The visual fields, ERGs, and mfERGs were recorded not only from the affected eye but also from the fellow eye. These examinations were performed and analyzed by trained personnel who were masked to the condition of the eyes.

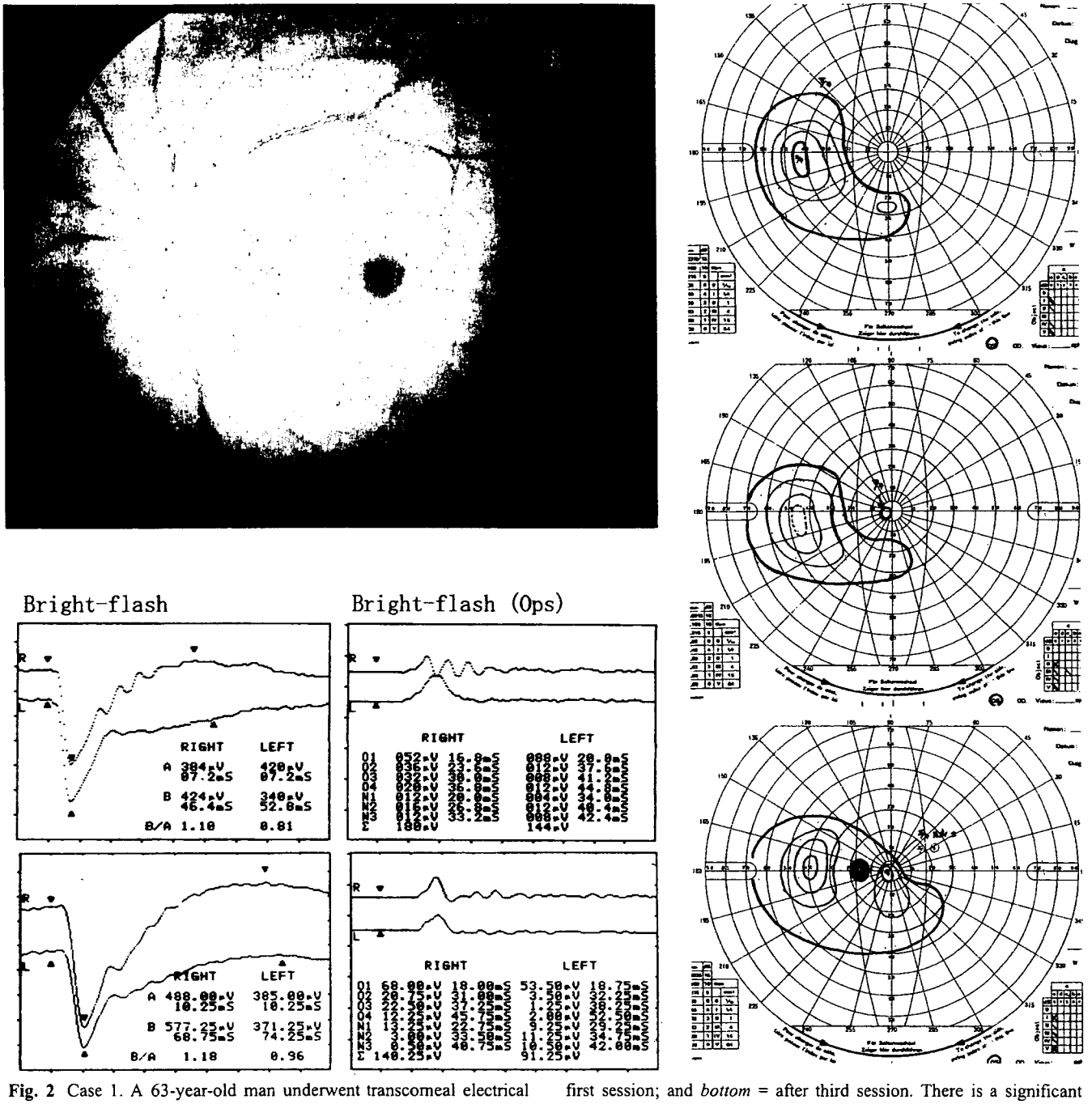

Fig. 2 Case 1. A 63-year-old man underwent transcorneal electrical retinal stimulation (TES) on his left eye 33 months after a central retinal artery occlusion (CRAO). *Top left:* Fundus photograph at the onset. *Right:* Goldmann visual fields: *top* = pre-TES; *middle* = after first session; and *bottom* = after third session. There is a significant improvement after the treatments. *Bottom left:* Full-field electroretinograms: *top* = pre-TES; *bottom* = post-TES. No significant change can be seen

Results

All of the patients reported perceiving phosphenes during the TES indicating that the visual system had been activated. The threshold currents to elicit phosphene are shown in Table 1. After treatment, all the patients reported their subjective sensations. Case 1 reported that the visual field in the affected eye expanded, and Case 2 reported that the central scotoma in the affected eye became smaller and the black spot in the central visual field became less dark. Case 3 reported that the visual field in the nasal inferior quadrant, which was dark, became lighter and clearer after TES. All three patients requested a continuation of the TES.

The Goldmann perimetric fields determined before and after treatment for each case are shown in Figs. 2, 3, and 4. In Case 1, a small peripheral island was present pre-TES, and after the first session of the TES, a small central island was detected connected to the original peripheral island. In

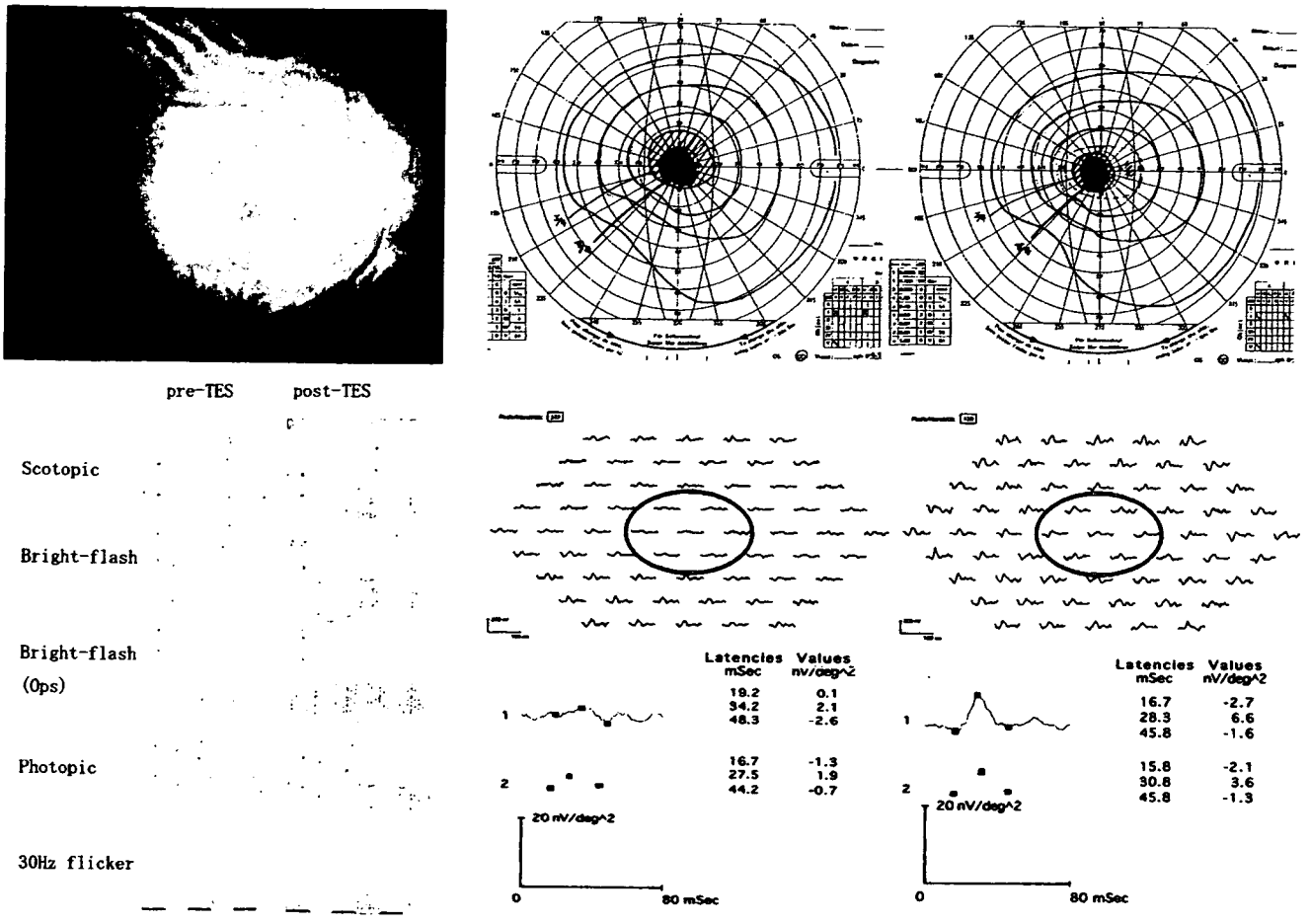

Fig. 3 Case 2. A 49-year-old man underwent transcorneal electrical retinal stimulation (TES) therapy in the right eye 15 months after central retinal artery occlusion (CRAO). *Top left:* Fundus photograph at the onset. *Top right:* Goldmann visual fields showing that the relative and absolute central scotomata became smaller after the treatment. *Left* = pre-TES; *right* = after-TES. *Bottom left:* Full-field electroretinograms showing significant improvement in the photopic and 30 Hz flicker ERGs. *Bottom right:* Multifocal electroretinograms showing increased responses in the central (area 1) and peripheral (area 2) retinal areas

Case 2, the central relative or absolute scotoma became smaller after the TES. In Case 3, the borders of all isopters were expanded.

In Case 1, the best-corrected visual acuity in the affected eye before treatment was 0.09, and it was 0.15 after treatment. Similarly in Case 2, the best-corrected visual acuity in the affected eye before treatment was 0.06 and was 0.15 after treatment, and in Case 3 the visual acuity was 1.2 before treatment and was the same after the TES.

The amplitude of each electroretinogram (ERG) component is shown in Table 2. The full-field ERGs after the TES in Case 2 were markedly improved, especially the cone and flicker ERGs (Fig. 3). In the other two cases, the changes were not remarkable (Figs. 2 and 4). The mfERGs that had been reduced in the areas corresponding to the ischemic retinal areas were improved after the TES in Cases 2 and 3 (Figs. 3 and 4). In Case 2, the averaged response from areas 1 and 2 is shown in Fig. 3. The N1-P1 amplitude and the P1 latency were improved after TES treatment. The N1-P1 amplitude and the P1 latency from each ring (ring 1 to 5) which is defined as default setting in the software from central to periphery are shown in Table 3. The N1-P1 amplitude significantly increased (paired t-test, $P<0.05$), and the P1 latency did not change significantly (paired t-test, $P>0.05$) after TES treatment. In Case 3, the averaged response from areas 1 and 2 is shown in Fig. 3. The N1-P1 amplitude from area 2 increased, whereas the amplitude from area 1 did not change after TES. The P1 latency from area 2 became shorter after treatment, whereas that from area 1 did not change. The averaged N1-P1 amplitude and the P1 latency from individual 16 hexagonal areas from areas 1 and 2 (see Fig. 4) are shown in Table 4. The N1-P1 amplitude from area 2 significantly increased (paired t-test, $P<0.05$), whereas the amplitude from area 1 did not change after treatment (paired t-test, $P>0.05$). The P1 latency from each area did not change after treatment (paired t-test, $P>0.05$).

All patients showed a transient superficial keratitis just after each treatment, otherwise there were no obvious changes by slit-lamp examinations and ophthalmoscopy. No systemic complications were observed.

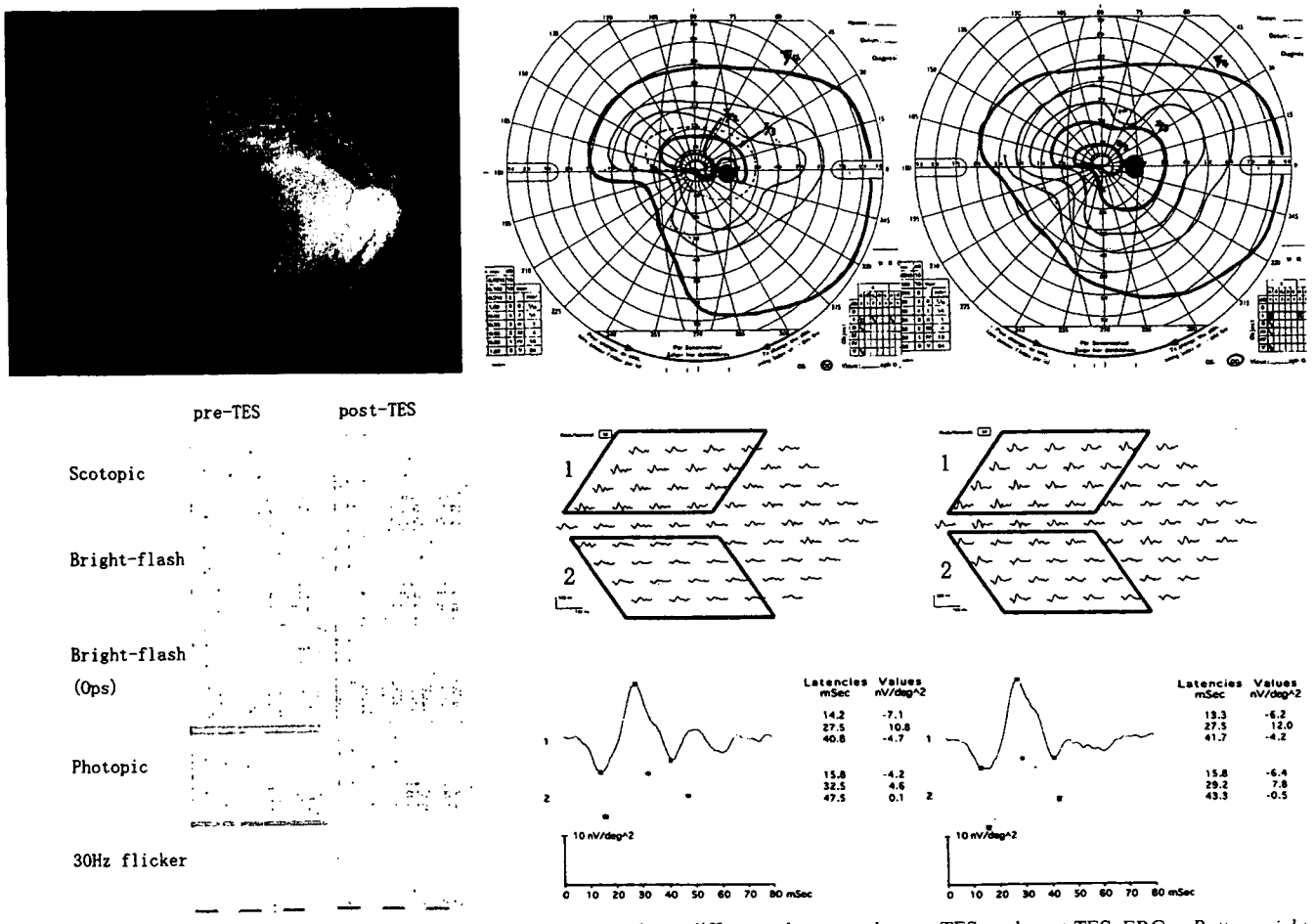

Fig. 4 Case 3. A 38-year-old woman underwent transcorneal electrical retinal stimulation (TES) on her right eye 26 months after a branch retinal artery occlusion (BRAO). *Top left:* Fundus photograph before the treatment. *Top right:* Goldmann visual fields showing that each isopter is larger after the treatment. *Left* = pre-TES; *right* = post-TES. *Bottom left:* Full-field electroretinograms showing no significant difference between the pre-TES and post-TES ERGs. *Bottom right:* Multifocal electroretinograms showing an increase in the response which had been reduced in the ischemic retinal area (area 2) compared with the area (area 1) symmetrical to area 2 against a horizontal meridian

Table 2 The amplitude of each ERG component

			Scotopic		Bright-flash			Photopic	Flicker
			b wave	a wave	b wave	b/a ratio	Sum of ops	b wave	
Case 1	R(healthy)	pre	-	384	424	1.10	180	-	-
		post	-	488	577	1.18	140	-	-
	L(diseased)	pre	-	420	340	0.81	144	-	-
		post	-	385	371	0.96	91.25	-	-
Case2	R(diseased)	pre	233.5	279	355.5	1.27	125	52.5	25.5
		post	205	359	443.25	1.23	118.5	80	54.25
	L(healthy)	pre	321.25	360.5	408.25	1.13	189.75	118	75.25
		post	256.25	376.5	534.5	1.42	130.75	121	84
Case3	R(diseased)	pre	173.75	425	531	1.25	157.75	91	44.25
		post	213.25	440	478	1.09	225	148	43.25
	L(healthy)	pre	365.25	515	663.25	1.29	309.25	176	114.75
		post	288.25	466	547	1.17	252.75	214	108.25

Data are shown as absolute value (uV). Each raw response is shown in the Figs. 2, 3, and 4.

Table 3 Rring analysis of mfERG in case 2

	Averaged N1-P1 amplitude (nV/deg^2)*		Averaged P1 latency (ms) (N.S.)	
	pre TES	post TES	pre TES	post TES
Ring 1	4.4	14.7	25	27.5
Ring 2	2.7	9	34.2	28.3
Ring 3	3.7	6.6	26.7	30.8
Ring 4	2.9	5.9	30.8	30
Ring 5	2.9	5.6	27.5	30.8

ring 1–5 is determined in the VERIS Science 4.1.1
TES : transcorneal electrical retinal stimulation therapy
*: $p<0.05$, N.S.: not significant

Discussion

Hayreh et al. reported [2, 3] that the retinal survival time after complete CRAO was 240 minutes in old, atherosclerotic, and retinal hypertensive monkeys. In most patients with CRAO, however, the occlusion is usually not complete and is transient, and recirculation may take place resulting in some improvement of visual function [1, 9, 23–24]. Although such recovery of visual function depends on the severity of occlusion and treatment, the critical period of improvement is limited. Miyake et al. [7] reported that in cases of CRAO the critical period during which visual function can be recovered was 14 days, even with hyperbaric oxygen treatment. It has also been reported that significant visual loss persists in the majority of patients with CRAO, despite some maneuvers which are effective when applied in the acute phase of selected cases [1, 9, 23–24]. It was thus surprising that the visual function was still recoverable in eyes 15 to 33 months after RAO.

Electrical stimulation delivered by subretinal electrodes following axotomy in rats was reported to have a protective effect on the remaining retinal neurons, possibly by up-regulating neurotrophic factors [11]. However, the electrical stimulation was delivered 10 minutes after the axotomy. In our cases, the shortest interval between the RAO and TES was 15 months. Thus, our findings would indicate that electrical stimulation of the retinal neurons might have a neuroreactivative effect on the damaged retina.

Table 4 The individual hexagonal response from each area in case 3

	N1-P1 amplitude (nV/deg^2)		P1 latency (ms)	
	pre-TES	post-TES	pre-TES	post-TES
Area 1	20.11±4.37	21.49±5.04	27.19± 1.24	27.81± 1.18
Area 2	10.39*±3.92	16.53*±5.33	29.26± 2.86	29.95± 2.63

data are shown as mean ± SD
Area 1 is corresponding to the healthy inferior retinal region.
Area 2 is corresponding to the affected superior retinal region.
TES : transcorneal electrical retinal stimulation therapy, *: $p<0.01$

In the 1960s, a number of investigators reported on the use of electrical retinal stimulation in patients to evaluate the residual retinal function, but not for treatment [18–21]. In those studies, the electrical stimuli were delivered by corneal contact-lens electrodes, and no severe adverse effects were reported. Similarly, our patients under very similar experimental procedures did not have any serious adverse effects.

The mechanism for the reactivation of retinal neurons by TES has not been determined. Morimoto et al. reported that electrical stimulation rescued retinal ganglion cells function by activating an endogenous retinal IGF-1 system [13]. A therapeutic effect of TES has been reported in patients with nonarteritic ischemic optic neuropathy or traumatic optic neuropathy [22]. The marked deterioration of the subjective visual function in patients with RAO may result largely from the damage to ganglion cells [25]. Our findings can be explained in part by a restoration of the function of ganglion cells. The improvement of the ERGs also suggests some recovery of function distal to ganglion cells and visual field as well. Because of the small number of cases, it is not possible to determine which retinal layer was affected by the TES.

Our results demonstrated that electrical retinal stimulation has the potential of improving retinal function, even in longstanding cases of RAO. It is noteworthy that the improvement of visual function was indicated by ERGs objectively in the three cases. The responses of the fellow eye and the unaffected areas on the different days were repeatable, which indicated that the responses from the affected eye or affected area were reliable.

Fujikado et al. reported [22] that a single TES treatment was effective in improving vision up to 3 months, and this was suggested to be due to the up-regulation of IGF-1 in the rat retina up to 2 weeks after TES [13]. Our protocol of a 1-month interval of TES was chosen from their findings. Additional laboratory studies are needed to determine more conclusively the mechanism of the therapeutic effect of TES.

The contact-lens electrode we used was a modified Burian-Allen contact-lens electrode. Compared to these corneal contact electrodes, the DTL electrode [26] might have been better to use in TES therapy to apply the proper electrical current. This is because it is less troublesome to the patient and can thereby be better accepted, and second, it has recently been shown that it can evoke phosphenes safely, quickly, and reliably [27]. Further investigations on the practicability of the electrode would be helpful in establishing TES for clinical situations.

The information and results obtained from this study indicate the future possibility of TES for other refractory retinal disease. Further investigations on a larger number of

patients for a longer period are necessary. A randomized control trial, and also basic research, will be necessary to determine the feasibility of the therapy and to determine the underlying mechanism for the improvements induced by TES on severely damaged retinas.

References

1. Sharma S, Brown GC (2006) Retinal artery obstruction. In: Ryan SJ (ed) Retina, 4th edn. Mosby, Philadelphia, pp 1323–1338
2. Hayreh SS, Kolder HE, Weingeist TA (1980) Central retinal artery occlusion and retinal tolerance time. Ophthalmology 87:75–78
3. Hayreh SS, Zimmerman MB, Kimura A, Sanon A (2004) Central retinal artery occlusion. Retinal survival time. Exp Eye Res 78: 723–736
4. Ffytche TJ (1974) A rationalization of treatment of central retinal artery occlusion. Trans Ophthalmol Soc UK 94:468–479
5. Schmidt D (2000) Ocular massage in a case of central retinal artery occlusion the successful treatment of a hitherto undescribed type of embolism. Eur J Med Res 5:157–164
6. Schmidt D, Schumacher M, Wakhloo AK (1992) Microcatheter urokinase infusion in central retinal artery occlusion. Am J Ophthalmol 113:429–434
7. Miyake Y, Niimi K (1973) Hyperbaric oxygen therapy on retinal arterial occlusion. 5th International Hyperbaric Congress Proc 1: 500–510
8. Atebara NH, Brown GC, Cater J (1995) Efficacy of anterior chamber paracentesis and carbogen in treating nonarteritic central retinal arterial occlusion. Am J Ophthalmol 102:2029–2034
9. Augsburger JJ, Magargal LE (1980) Visual prognosis following treatment of acute retinal artery obstruction. Br J Ophthalmol 64: 913–917
10. Fraser S, Siriwardena D (2002) Interventions for acute non-arteritic central retinal artery occlusion. Cochrane Database Syst Rev. CD001989
11. Morimoto T, Miyoshi T, Fujikado T, Tano Y, Fukuda Y (2002) Electrical stimulation enhances the survival of axotomized retinal ganglion cells in vivo. Neuroreport 13:227–230
12. Chow AY, Chow VY, Packo KH, Pollack JS, Peyman GA, Schuchard R (2004) The artificial silicon retina microchip for the treatment of vision loss from retinitis pigmentosa. Arch Ophthalmol 122:460–469
13. Morimoto T, Miyoshi T, Matsuda S, Tano Y, Fujikado T, Fukuda Y (2005) Transcorneal electrical stimulation rescues axotomized retinal ganglion cells by activating endogenous retinal IGF-1 system. Invest Ophthalmol Vis Sci 46:2147–2155
14. Nibuya M, Morinobu S, Duman RS (1995) Regulation of BDNF and trkB mRNA in rat brain by chronic electroconvulsive seizure and antidepressant drug treatments. J Neurosci 15:7539–7547
15. Al-Majed AA, Brushart TM, Gordon T (2000) Electrical stimulation accelerates and increases expression of BDNF and trkB mRNA in regenerating rat femoral motoneurons. Eur J Neurosci 12:4381–4390
16. Pardue MT, Phillips MJ, Yin H et al (2005) Neuroprotective effect of subretinal implants in the RCS rat. Invest Ophthalmol Vis Sci 46:674–682
17. Pardue MT, Phillips MJ, Yin H, Fernandes A, Cheng Y, Chow AY, Ball SL (2005) Possible sources of neuroprotection following subretinal silicon chip implantation in RCS rats. J Neural Eng 2: S39–S47
18. Potts AM, Inoue J, Buffum D (1968) The electrically evoked response of the visual system (EER). Invest Ophthalmol 7:269–278
19. Miyake Y, Yanagida K, Yagasaki K (1980) Clinical application of EER (electrically evoked response). (1) Analysis of EER in normal subjects (author's transl). Nippon Ganka Gakkai Zasshi 84:354–360 (Japanese)
20. Miyake Y, Yanagida K, Yagasaki K (1980) Clinical application of EER (electrically evoked response) (2) Analysis of EER in patients with dysfunctional rod or cone visual pathway (author's transl) Nippon Ganka Gakkai Zasshi 84:502–509 (Japanese)
21. Shimazu K, Miyake Y, Watanabe S (1999) Retinal ganglion cell response properties in the transcorneal electrically evoked response of the visual system. Vision Res 39:2251–2260
22. Fujikado T, Morimoto T, Matsushita K, Shimojo H, Okawa Y, Tano Y (2006) Effect of transcorneal electrical stimulation in patients with nonarteritic ischemic optic neuropathy or traumatic optic neuropathy. Jpn J Ophthalmol 50:266–273
23. Gold D (1977) Retinal arterial occlusion. Trans Am Acad Ophthalmol Otolaryngol 83:392–408
24. Atebara NH, Brown GC, Cater J (1995) Efficacy of anterior chamber paracentesis and Carbogen in treating acute nonarteritic central retinal artery occlusion. Ophthalmology 102:2029–2035
25. Miyake Y (2006) Central reinal artery occlusion in electrodiagnosis of retinal diseases. Springer-Verlag, Tokyo, pp 181–182
26. Dawson WW, Trick GL, Litzkow CA (1979) Improved electrode for electroretinography. Invest Ophthalmol Vis Sci 18:988–991
27. Gekeler F, Messias A, Ottinger M, Bartz-Schmidt KU, Zrenner E (2006) Phosphenes electrically evoked with DTL electrodes: a study in patients with retinitis pigmentosa, glaucoma, and homonymous visual field loss and normal subjects. Invest Ophthalmol Vis Sci 47:4966–4974

GRAA_245_12_2007610

Transient macular dysfunction determined by focal macular electroretinogram

Rapid diagnosis of patients with acute visual loss is critical[1] but is difficult if the retina appears normal ophthalmoscopically. We report the case of a patient who presented with acute unilateral visual loss and a central scotoma.

Case report

A 75-year-old man complained of a sudden and painless decrease of vision in his left eye. He had undergone surgery for an unruptured intracranial aneurysm 20 years earlier and was taking 7 mg/day of systemic prednisolone for rheumatoid arthritis. He had also had diabetic mellitus without retinopathy for 5 years. He was being followed for a left hemianopsia and normal tension glaucoma for the previous 3 years.

On examination, a left relative afferent papillary defect (RAPD) was observed, and visual acuity (VA) was 20/30 OD and 20/2000 OS. All of the ocular findings were normal except for enlarged disc cupping OU (fig 1). Fluorescein angiography showed a delay in the arm-to-retina circulation time of 20.0 s (fig 1). Neither retinal emboli nor localised filling delay were observed. Goldmann perimetry showed a left quadrantic homonymous hemianopsia and a small central scotoma with peripheral constriction. The alterations in the left eye were new (fig 1). Focal macular electroretinograms (FMERGs) were recorded 2 h after onset as described (see the supplemental figure available at http://bjo.bmj.com/supplemental).[2 3]

The FMERGs were decreased in the left eye (fig 2) indicating that the visual dysfunction was retinal in origin. Left VA improved to 20/250 spontaneously 3 h later. On the following day, VA had improved to 20/30, and the amplitudes of the FMERGs, full-field ERGs and pattern visual evoked response (VEP) were normal (fig 2). The visual field obtained 3 months later showed that the central scotoma was not present and an expansion of the peripheral visual fields (fig 1). The fundus remained normal. Ultrasound echography revealed no stenosis of the carotid artery. Blood examination revealed rheumatoid factor and high HbA1c but was otherwise normal.

We conclude that the acute visual loss and central scotoma with reduced FMERGs were consistent with transient macular ischaemia, and prophylactic anti-coagulation treatment was considered.

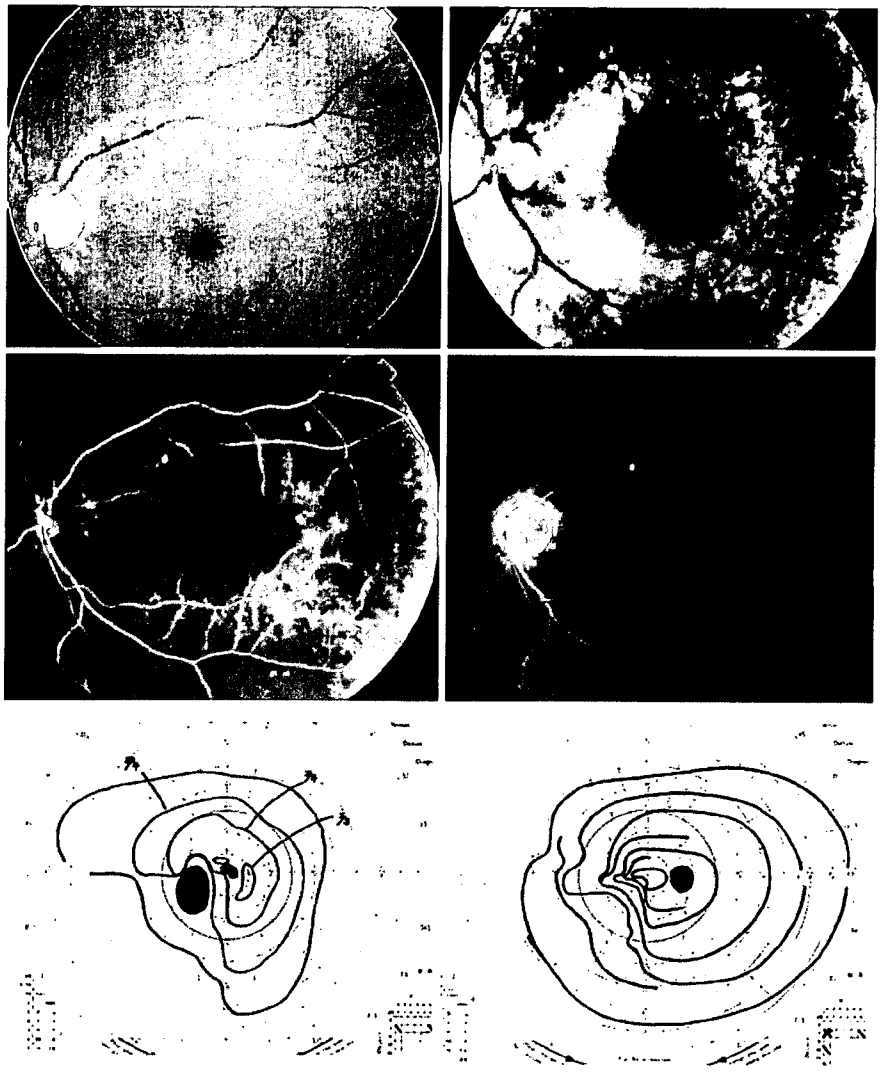

Figure 1 Fundus photograph and fluorescein fundus angiograms of the patient's left eye. Top left: Fundus photograph showing enlarged cupping of the left optic disc. Top right: Fluorescein angiogram with delayed arm-to-retina circulation time. Second left and right: Fluorescein angiogram showing neither localised arteriolar filling delay nor retinal emboli in the middle (left) and late (right) phases. Third left: Goldmann visual field in the acute phase shows small central scotoma and peripheral constriction in addition to a decrease in the isopters in the left temporal inferior area (quadrantic homonymous hemianopsia) which had existed for years in the left eye. The central scotoma and peripheral constriction were new. Visual acuity (VA) was 20/2000 OS. Third right: Goldmann visual field performed 6 months earlier showing a decrease in the isopters in the left nasal inferior area (homonymous hemianopsia) in the right eye. VA was 20/30 OD. Bottom: Goldmann visual field performed 3 months after the onset showing disappearance of the central scotoma and an improvement of peripheral isopters. VA was 20/30 OS.

Comments

Our patient had an acute monocular visual loss and a fundus that appeared normal except for the relatively delayed angiographic retinal filling time and enlarged disc cups. The RAPD, central scotoma and systemic complications made it difficult to determine the site of the alterations. The reduced FMERGs pointed to the retina as the site.

However, an abnormally long-lasting visual decrease is not typical for amaurosis fugax,[1] and ophthalmoscopy did not show retinal oedema typical of arteriolar occlusion. Conventional electrophysiological examinations such as full-field ERGs and VEPs might be useful except when the ischaemic site is in the macular region.

The clinical course in our case was compatible with a transient retinal ischaemia with a possibility of a transient central retinal artery occlusion, although additional more generalised abnormalities cannot be completely excluded. The FMERG within the 5° area is similar to that of the ERG of a monkey treated with 2-amino-4-phosphonobutyric acid (APB) and cis-2,3-piperidine dicarboxylic acid (PDA) to suppress both on and off synapses.[4 5] This implies that the inner retinal layers have serious dysfunction. Because of the systemic complications, the risk of utilising prophylactic anticoagulant agents was discussed. However, the VA and central scotoma quickly recovered accompanied by an improvement in the FMERGs without any intervention.

These findings indicate that clinicians should consider focal macular dysfunction in cases of acute vision loss and normal retinal appearance; multifocal ERGs or FMERGs are useful in determining the site of the pathology. 1

Acknowledgements

This study was supported by the Suzuken Memorial Foundation.

Naoki Terauchi, Kaoru Fujinami, Kei Shinoda, Kazushige Tsunoda, Gen Hanazono, Koichi Inomata, Yozo Miyake

Laboratory of Visual Physiology, National Institute of Sensory Organs, National Hospital Organization, Tokyo Medical Center, 2-5-1 Higashigaoka, Meguro-ku, Tokyo 152-8902, Japan

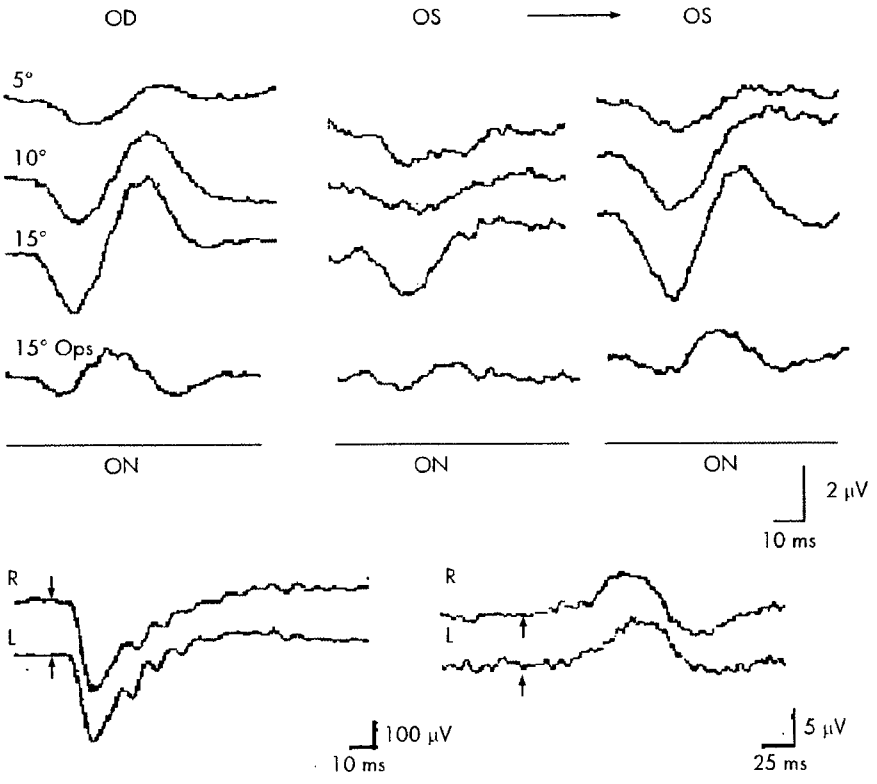

Figure 2 Focal macular electroretinogram (FMERG, top), full field electroretinogram and visual evoked response (VEP) from both eyes (bottom). Top: Upper three recordings show the photopic a- and b-waves, and lowest recordings show the oscillatory potentials (Ops). The stimulus spot size was 5°, 10° and 15° as indicated in the figure. Left and centre: FMERGs recorded during the acute phase. The ERGs of the left eye (centre) are reduced compared with those of the right eye. Right: FMERGs recorded on the following day showing the recovery of all components of the left eye. The a-wave is not affected as much as the b-waves and Ops. Bottom left: Bright-flash ERG showed no significant difference in the two eyes even in the oscillatory potentials which are sensitive to retinal ischaemia. Bottom right: The VEPs showed no significant difference between the two eyes. The stimulus onset of full field ERG and VEP is indicated by arrows.

Naoki Terauchi
Department of Ophthalmology, Keio University, School of Medicine, 35 Shinanomachi, Shinjuku-ku, Tokyo 160-8582, Japan

Koichi Inomata
Department of Ophthalmology, School of Medicine, Nihon University, 1-8-13 Surugadai, Kanda, Chiyoda-ku, Tokyo 101-8309, Japan

Correspondence to: Dr Kei Shinoda, Laboratory of Visual Physiology, National Institute of Sensory Organs, National Hospital Organization, Tokyo Medical Center, 2-5-1 Higashigaoka, Meguro-ku, Tokyo 152-8902, Japan; shinodakei@kankakuki.go.jp

doi: 10.1136/bjo.2006.113373

Accepted 3 February 2007

Competing interests: None of the authors have any financial or proprietary interest in any material or methods mentioned.

The supplemental figure is available at http://bjo.bmj.com/supplemental.

References

1 **Rizzo III JF.** Neuroophthalmologic disease of the retina. In: Daniel MA, eds. *Principles and practice of ophthalmology*, 2nd ed. Philadelphia: WB Saunders, 2000:4083–108.
2 **Miyake Y,** Shiroyama N, Horiguchi M, *et al.* Oscillatory potentials in electroretinograms of the human macular region. *Invest Ophthalmol Vis Sci* 1988;**29**:1631–5.
3 **Miyake Y.** Focal macular ERGs. In: Miyake Y, eds. *Electrodiagnosis of retinal diseases.* Tokyo: Springer, 2005:20–32.
4 **Ueno S,** Kondo M, Niwa Y, *et al.* Luminance dependence of neural components that underlies the primate photopic electroretinogram. *Invest Ophthalmol Vis Sci* 2004;**45**:1033–40.
5 **Sieving PA,** Murayama K, Naarendorp F. Push-pull model of the primate photopic electroretinogram: a role for hyperpolarizing neurons in shaping the b-wave. *Vis Neurosci* 1994;**11**:519–32.

最近のトピックス

網膜内因性信号測定装置

（東京医療センター臨床研究センター，理化学研究所脳統合機能研究チーム）　花園　元
（（株）ニデック）　柴田　尚久
（（株）ニデック）　楠城　紹生
（理化学研究所脳統合機能研究チーム）　谷藤　学
（東京医療センター臨床研究センター，理化学研究所脳統合機能研究チーム）　角田　和繁

1. はじめに

眼科における画像診断技術は近年，目覚ましい進歩をとげてきた。たとえば光干渉断層計（以下OCT）は，検眼鏡によって捉えることのできない網膜微細構造の観察を可能にするものであり，網膜疾患の診断，治療に関する従来の常識を一変させるほど臨床応用価値の高いものである。しかしOCTや，走査型レーザー検眼鏡（SLO）などの画像診断法は解剖学的構造の把握を目的としており，これによって視細胞をはじめとする網膜の神経活動を捉えることはできない。したがって，網膜機能（神経活動）の他覚的評価のためには，電気生理学的検査である網膜電図（ERG）が今でも主要な役割を果たしている。

我々のグループでは，神経活動に伴って組織の光反射率が変化する現象を利用した計測法（内因性信号計測法）を眼底に応用し，網膜の神経活動を非侵襲的にイメージングする方法を開発することに成功した（網膜内因性信号測定装置：Functional Retinography）。

2. 測定原理

網膜内因性信号測定装置では，神経活動に伴って神経組織の微細構造や光反射率が変化する現象を利用している。実際の計測法は，神経組織をcharge-coupled device（以下CCD）カメラでイメージングし，刺激前と刺激後の画像を重ね合わせて比較するという非常に単純なものである。刺激後に画像の明るさが変化している部分が神経活動の起きた領域に相当し，通常は神経活動の高い領域がより暗くみえる（図1）。

図1　内因性信号の計測方法

3. 測定方法

開発のための動物実験では，ヒトとほぼ同じ解剖学的構造をもつニホンザル，アカゲザルの眼底を用いている。全身麻酔下において非動化した眼底を，ニデック製眼底カメラを改良した観察系を用いて

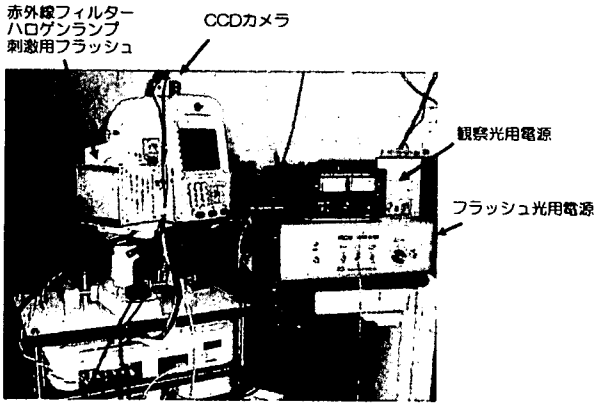

図2　網膜内因性信号計測装置の外観

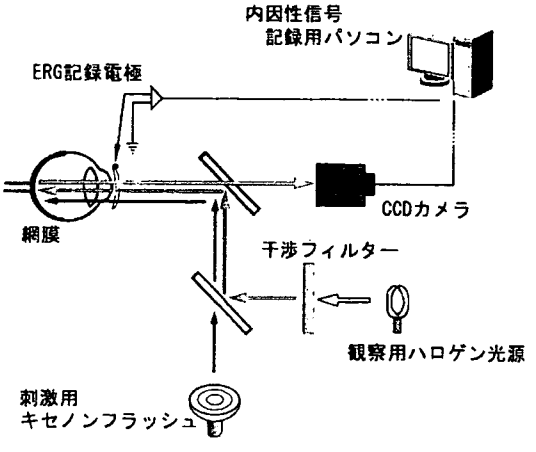

図3　網膜内因性信号計測装置の概要

CCDカメラでモニターする（図2，3）。眼底観察用のハロゲン光は，赤外線フィルターを透過して眼底後極部を照明する。解像度640×480ピクセル，毎秒30フレームのCCDカメラによって眼底からの光反射率変化を持続的に記録する。測定開始から0.5秒後に眼底後極部全体を白色キセノンフラッシュにて刺激する。1回の測定は通常5～10秒間行う。

刺激前0.5秒間の平均画像の反射率と，刺激後の画像における反射率との比をピクセルごとに計算し，その比を256階調にスケーリングし画像化する（図4）。

4. 測定結果

フラッシュによるびまん性刺激によって視細胞が活動すると，網膜全体の反射率が低下し画像では黒く描出される。この内因性信号は刺激後150 msecにピークをもつ早い反応で，中心窩で最も強い。信号強度を疑似カラーで表示すると，明順応下では中心窩に内因性信号の急峻なピークを認め，周辺部に向かって減少する（図5）が，暗順応下では中心窩に加えて周辺部にドーナツ状のピークを認める（図6）。内因性信号のピークは中心窩では錐体視細胞に，周辺部では桿体視細胞の解剖学的な分布によく一致しており，網膜内因性信号は網膜外層の機能をよく反映していると思われた。

更に視神経乳頭部に注目すると，ここでは網膜面とは異なりフラッシュ刺激後にゆっくりと信号が強くなっていく。これは刺激後の血流増加を反映した光散乱強度変化と考えられ，中心動静脈に相当する視神経乳頭中央部に急峻なピークがみられる（図7）。

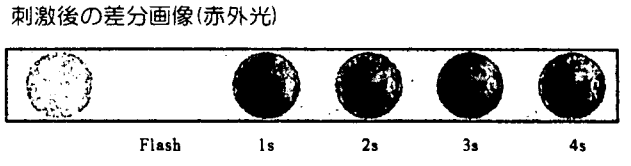

図4　内因性信号の時間経過

5. 網膜内因性信号のバリエーション

前項では，観察光として赤外光，刺激としてびまん性フラッシュ刺激を用いた例を挙げてきたが，網膜内因性信号計測装置は，測定条件・刺激条件を様々に変化させることで信号起源の異なる反応を測定することができる。

1）局所刺激による内因性信号

網膜内因性信号計測装置の眼底網膜との共役面にフィルターを設置することで局所フラッシュ刺激を

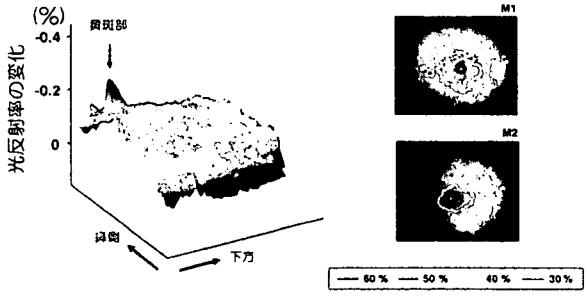

図5　明順応下での網膜内因性信号の三次元トポグラフィ

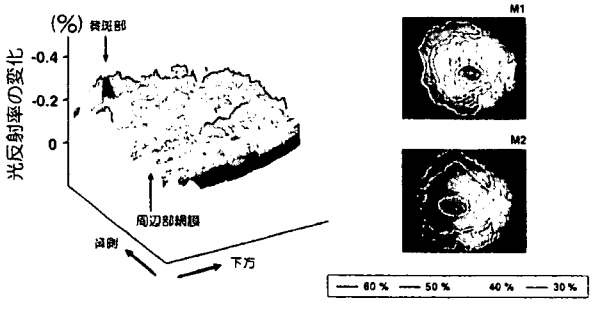

図6　暗順応下での網膜内因性信号の三次元トポグラフィ

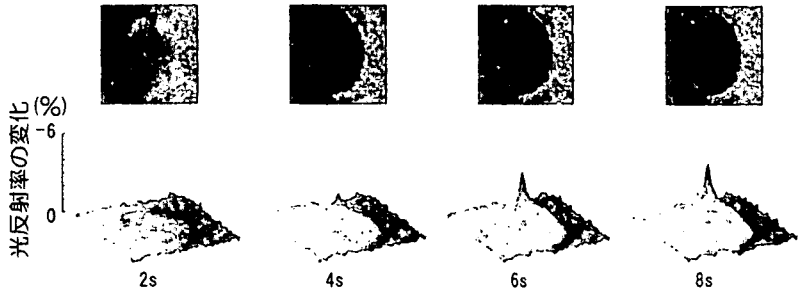

図7　視神経乳頭部の内因性信号の三次元トポグラフィ

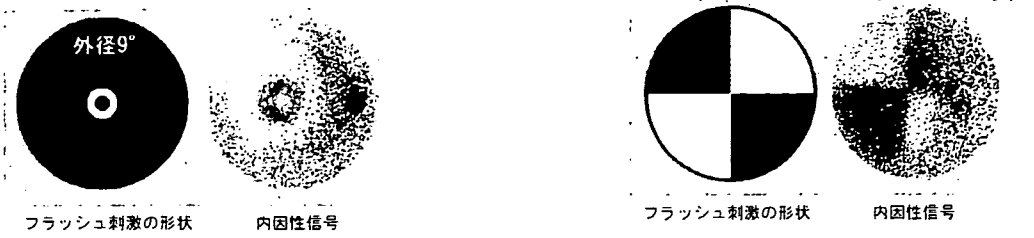

図8　フラッシュ部分刺激に対する内因性信号

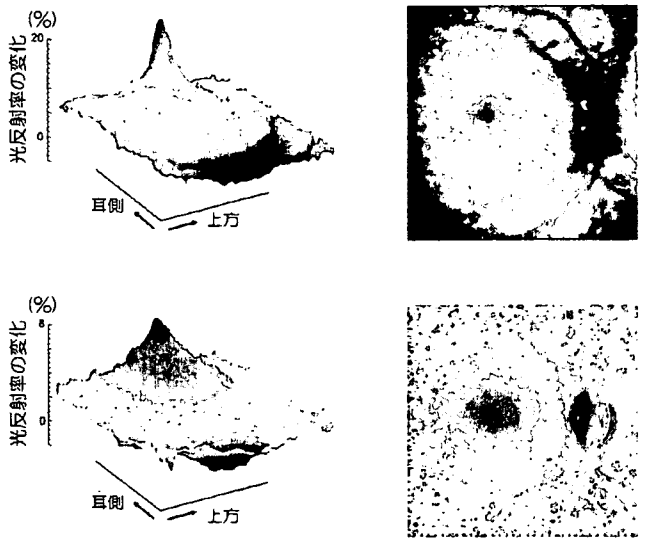

図9　カラーフィルターを用いて測定した褪色反応のトポグラフィ（上：570nm　下：630nm）

行うことができる。刺激部位に相当する網膜のみから内因性信号が記録される（図8）。

2）可視光を用いた眼底観察による内因性信号

眼底観察光として可視光を用いることで視細胞外層の色素褪色変化（bleaching）を捉えることができる。これは，赤外光での内因性信号の測定とは異なり，褪色変化が起きた部分の網膜の反射率が上がる（明るくなる）反応であるが，630 nm の観察光では5%以上，570 nm の観察光では10%以上の大きな反射率変化が中心窩において認められる（図9）。

3）経強膜電気刺激による内因性信号

経強膜電気刺激により電気的に網膜を刺激し内因性信号を測定すると，フラッシュ刺激でみられた中心窩の信号ピークがみられず，網膜後極部全域でほぼ同程度の内因性信号がみられた。信号分布は明順応および暗順応の状態でも変わりはなく，信号発生の起源として網膜内層の寄与が大きいと思われる。

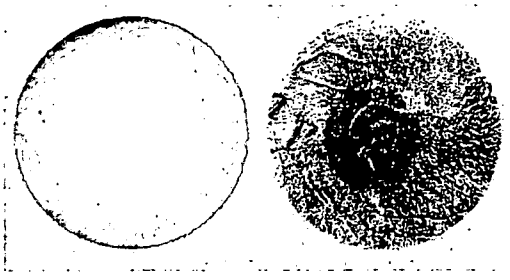

図10　フラッシュ部分刺激に対する内因性信号（ヒト網膜，覚醒下）

6. ま と め

網膜内因性信号計測装置の原理・測定方法および可能性について測定結果を挙げて述べた。覚醒下のヒトでは，測定は可能なものの動物眼ほどの安定した結果を得るには至っていない（図10）。しかし近い将来臨床応用が実現すれば，網膜神経機能の客観的な評価法として疾患の早期発見や早期治療につながることが期待される。

参 考 文 献

1) Tsunoda K, Oguchi Y et al : Mapping cone- and rod-induced retinal responsiveness in macaque retina by optical imaging. Invest Ophthalmol Vis Sci 45: 3820-3826, 2004.
2) Hanazono G, Tsunoda K et al : Intrinsic signal imaging in macaque's retina reveals different types of flash-induced light reflectance changes of different origins. Invest Ophthalmol Vis Sci, in press.

シンポジウム1：分子生物と電気生理

網膜内因性信号計測法

－Functional Retinography (FRG)－

角田和繁

東京医療センター感覚器センター・理化学研究所脳科学総合研究センター

Intrinsic Signal Imaging of the Retina

- Functional Retinography (FRG) -

Kazushige Tsunoda

National Institute of Sensory Organs, Laboratory of Visual Physiology and RIKEN Brain Science Institute

我々は網膜の神経機能を非侵襲的に画像化する方法を開発し，新たな眼科診断機器としての実用化に向けた研究を行っている（網膜内因性信号計測法，functional retinography：FRG）。この方法が実用化されれば，網膜生理現象の更なる解明および病態網膜における機能的マッピングが可能となり，網膜疾患についての更に確実な診断情報を提供してくれるものと期待される。

（眼　紀　58：477－478，2007）

キーワード：網膜内因性信号計測法，光学計測法，網膜機能的イメージング

We are developing a new imaging system called functional retinography (FRG) that will be able to measure neural activity in the retina non-invasively. We believe that FRG is the next step in furthering investigations into basic retinal physiology and also in the development of diagnostic tools for early identification of minor retinal dysfunction using non-invasive means.

(Folia Ophthalmol Jpn 58：477－478，2007)

Key Words : Intrinsic Signal Imaging, Optical Imaging, Retinal Function

緒　　言

眼科における画像診断技術は目覚ましく，とくに光干渉断層計（以下 OCT）は網膜疾患の診断，治療に関する従来の常識を一変させるほど臨床応用価値の高いものであった。しかし OCT，走査レーザー検眼鏡（SLO）などの画像診断法は解剖学的構造の把握を目的としており，視細胞をはじめとする網膜の神経活動を捉えることはできない。したがって，網膜機能（神経活動）の他覚的評価のためには，電気生理学的検査である網膜電図（以下 ERG）が最も主要な役割を果たしている。

我々は，ERG とは全く異なるしくみで，網膜の神経活動を非侵襲的にイメージングする方法（網膜内因性信号計測法，functional retinography 以下 FRG）を開発し，新たな眼科診断機器としての実用化に向けた研究を行っている。これは，神経活動に伴う代謝変化などを神経組織の光反射率変化として捉える計測法であり，近赤外光で眼底後極部をモニターした上で，フラッシュ刺激前後の画像を比較するという非常に単純なものである。アカゲザルを用いた実験では，中心窩における錐体視細胞の活動ピークや，血管アーケード付近の杆体視細胞の活動ピーク（rod ring）などを明瞭にマッピングできること[1]（図1），信号の閾値が ERG における暗順応 b 波と同等に低いこと[2]などが明らかになっている。そのほかにも空間分解能が高いこと（図2），非侵襲的であること，測定時間が短いことなどの利点があり，将来は本計測法を様々な網膜疾患の診断のための機能的マッピングに応用できる可能性がある。

また，本来 FRG は視細胞の機能的マッピングを目的としていたが，最近では網膜血流を反映した遅い信号成分を抽出することにより，網膜神経節細胞を中心とした網膜内層機能のマッピングが可能であることも示されている。

一方，最近では OCT 技術を利用して網膜神経活動を可視化する方法（functional OCT）についての研究も世界的に行

別刷請求先：152-8902 東京都目黒区東が丘 2-5-1　東京医療センター感覚器センター　角田和繁

Reprint requests to: Kazushige Tsunoda, MD　National Institute of Sensory Organs, Laboratory of Visual Physiology 2-5-1 Higashigaoka, Meguro-ku, Tokyo 152-8902, Japan

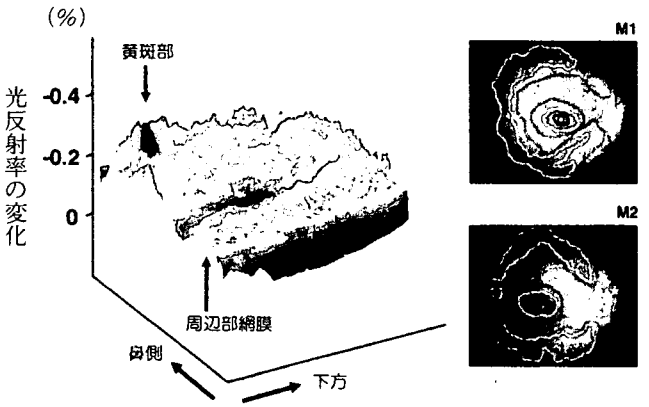

図1 びまん性フラッシュ刺激に対する暗順応下での functional retinography (FRG) トポグラフィ
——：60%，——：50%，　　：40%，——：30%

われている[3,4]。このように，網膜の神経機能をイメージングする技術は網膜の画像診断における新しい方向性であり，将来ヒトにおいて FRG 計測が可能になれば，網膜疾患についての更に確実な診断情報を提供してくれるものと期待される。

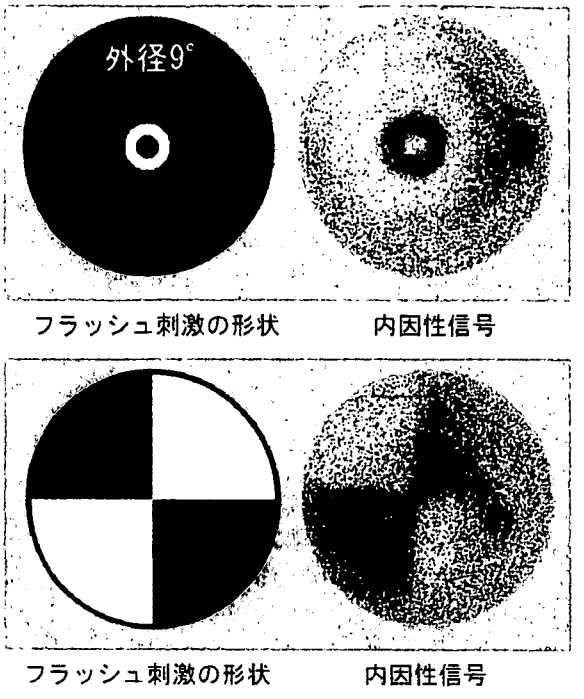

図2 局所フラッシュ刺激に対する FRG 信号

文　献

1) Tsunoda K, Oguchi Y et al : Mapping cone- and rod-induced retinal responsiveness in macaque retina by optical imaging. Invest Ophthalmol Vis Sci 45 : 3820-3826, 2004.
2) Hanazono G, Tsunoda K et al : Intrinsic signal imaging in macaque retina reveals different types of flash-induced light reflectance changes of different origins. Invest Ophthalmol Vis Sci 48 : 2903-2912, 2007.
3) Maheswari RU, Takaoka H et al : Novel functional imaging technique from brain surface with optical coherence tomography enabling visualization of depth resolved functional structure in vivo. J Neurosci Methods 124 : 83-92, 2003.
4) Srinivasan VJ, Wojtkowski M et al : In vivo measurement of retinal physiology with high-speed ultrahigh-resolution optical coherence tomography. Optics letters 31 : 2308-2310, 2006.

(2007年8月22日受付)

Functional optical coherence tomography reveals localized layer-specific activations in cat primary visual cortex in vivo

Uma Maheswari Rajagopalan* and Manabu Tanifuji

Integrative Neural Systems Lab., Brain Science Institute, RIKEN, 2-1 Hirosawa, Wako Shi, Saitama Ken, Japan
**Corresponding author: uma@brain.riken.go.jp*

Received January 19, 2007; revised June 13, 2007; accepted June 21, 2007;
posted July 17, 2007 (Doc. ID 79142); published August 28, 2007

Surface neural activity has been widely visualized using optical intrinsic signal imaging (OISI) from various cortical sensory areas. OISI of the cortical surface with a CCD camera gives integrated information across a depth of a few hundred micrometers. We visualize depth-resolved activation patterns of cat primary visual cortex by functional optical coherence tomography (fOCT). A comparison of the depth-integrated results of fOCT maps with the optical intrinsic signal profiles shows fairly good agreement. Our results reveal layer-specific activation patterns and indicate that the activation was not homogeneous. © 2007 Optical Society of America

OCIS codes: 170.4500, 110.1650, 330.4270, 000.1430, 330.4300, 030.5290.

Optical intrinsic signal imaging (OISI) is a popular functional mapping technique to obtain high-resolution brain activation maps in animal models [1]. OISI in principle measures the reflectance changes from the cortex of the brain and has revealed organization of clustering of neurons having similar response properties called columns with dimensions around a few hundred micrometers [2,3].

In OISI, the cortical surface under activation by stimulation is illuminated with visible light and is imaged onto a CCD camera. Through this approach, OISI can monitor the concentration of oxy–deoxyhemoglobin of blood as changes in absorption and structural changes as changes in scattering. As the detection process is done with a CCD camera, the measured reflected light is actually integration of reflections over the depth determined by the collection optics. In other words OISI is suitable for detection of clustered activation of neurons. In contrast, anatomically most of the cortex is a layered organization consisting of six layers distinguished by cell types and density of cells [4]. As OISI detects the clustered activation, the potential difference in the layered organization across depth may go undetected.

Utilizing the potential of optical cohrence tomography (OCT) [5] in resolving depth structures and taking advantage of the scattering changes during neural activity, we proposed the use of OCT in depth-resolved functional imaging and successfully demonstrated it in cat visual cortex [6,7]. Recently, supporting evidence for the potential of OCT in functional studies of squid axon [8] and of retina [9–11] and in the rat [12] have been reported. Here, we have obtained depth-resolved functional maps of cat visual cortex by functional OCT (fOCT).

To correlate the fOCT maps with the neural activity maps, we compared the results with the OISI results. The OISI technique in conjunction with the direct measurement of electrical activity has revealed that OISI indeed detects population activity of neurons [13]. This fact justifies our comparison of fOCT maps with OISI. Indeed, a comparison of the integrated profiles obtained from fOCT maps correlates fairly well with the intensity profiles of the intrinsic maps.

We used a fiber based OCT imaging system consisting of a Mach–Zehnder type heterodyne interferometer (Fig. 1A). A broadband source with output power of 30 mW, central mean wavelength of 1.31 μm, and a spectral width of 50 nm was used. The sample arm viewing the animal side consists of an objective lens of numerical aperture 0.08 and was also fitted with a CCD camera. This allowed simultaneous viewing of the cortical surface with the introduction of visible light from an auxiliary laser source. The system has a depth resolution of 34 μm in free space and a spot size of 20 μm. The image acquisition rate was 2 Hz,

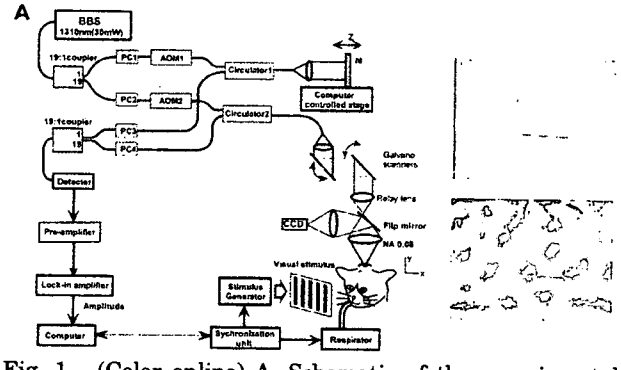

Fig. 1. (Color online) A, Schematic of the experimental system used. B, Exposed cortical surface of cat visual cortex and with C, an overlay of binarized activation map. BBS, broadband source; AOM, acousto-optic modulator; PC, polarization controller; M, mirror; O, objective lens. In C the dark and light patches represent, respectively, the activated regions for horizontal and vertical gratings, and the green lines indicate the region of the OCT scan. To reduce the respiratory fluctuation, data acquisition was done in synchronization with the heartbeat and respiration. The animal experimental protocol was approved by the Experimental Animal Committee of the RIKEN Institute, which follows the guidelines of the National Institutes of Health.

0146-9592/07/172614-3/$15.00

and each scan frame had 128×100 pixels over 1 mm transverse by 1 mm depth.

The fOCT experiments were conducted with anesthetized cats under artificial ventilation. The head of the animal was held tightly by attaching it to a metal rod. A stainless steel chamber was fixed onto the skull, and the inside of the sealed chamber was filled with agarose to keep the brain surface immobile. Figure 1B shows the exposed cortical surface with the clear blood vessels. The pupils of the eyes were dilated and fitted with contact lenses. The visual stimuli consisted of square-wave gratings presented in random on a CRT monitor. The stimuli consisted of five patterns with control or blank, horizontal (0°), vertical (90°), and oblique gratings (45°, 135°). A total of 40 trials were obtained for each stimulus. In a single trial, data acquisition was done for 8 s followed by a resting period of 5 s. Each trial period was 8 s with 2 s prestimulus and 6 s poststimulus durations. Stimulus duration was 2 s.

Prior to doing functional imaging with OCT, we performed OISI of the exposed cortical surface at a wavelength of 607 nm under identical stimulation conditions. OISI revealed that neurons responding to the same orientation are clustered and form an orientation map across the cortical surface. Figure 1C shows the binarized difference maps obtained when horizontal and vertical grating visual stimuli were presented to the cat. Dark and bright regions indicate the activated regions for horizontal and vertical gratings, respectively. An OCT x–z scan with an example as shown in Fig. 2A was done across the line indicated in the OISI map. The cortical surface border has been drawn manually, and the warm-colored regions indicate the scattering centers within the cortex. Following procedure had been applied to the OCT structural images before calculating the functional maps: (1) The scans were corrected for the misalignment of the surface position by use of a correlation-based procedure used previously [6]. (2) Pixel noise was removed with a smoothing filter of window size 27 μm×21 μm. Next, the ratio of the poststimulus over prestimulus scans for all four grating stimuli and the control condition where the control corresponds to blank screen condition was calculated as follows:

$$\gamma_s(x,d,t) = \frac{R_s^{post}(x,d,t)}{\sum_{prescans} R_s^{pre}(x,d,t)}. \quad (1)$$

Here R_s is the reflectivity at position (x,d) at time t. The superscripts *post* and *pre* indicate the poststimulus and prestimulus scans, respectively. The division operation removes the unchanging common variation and extracts only changes due to visual stimulation. Next, the ratio was averaged for all the scans obtained for each stimulus $\langle \gamma_s(x,d) \rangle$. Finally, the differential OCT signal $\langle \gamma_{diff}(x,d) \rangle$ was calculated as

$$\langle \gamma_{diff}(x,d) \rangle = \langle \gamma_{grating}(x,d) \rangle - \langle \gamma_{control}(x,d) \rangle. \quad (2)$$

With Eq. (2), by subtracting the differential OCT signal of the control, noise fluctuations such as respiration artifacts that were locked to the recording but not to the grating stimulus were removed. In this discussion, to make the comparison with OISI clearer and easier, we restrict ourselves mainly to the results obtained by calculating the difference $\langle \gamma_{diff}(x,d) \rangle$ obtained between two orthogonal gratings. The spatial map has been smoothed with a moving average filter of size around 100 μm×115 μm.

Figure 2B shows the calculated fOCT maps obtained as a difference of the fOCT maps obtained for horizontal and vertical grating stimuli. Here, red and blue patches indicate the activation for horizontal and vertical grating stimluli, respectively. In this pseudo-colored map, red means more scattering change for horizontal than for the vertical. In the corresponding intrinsic map of Fig. 1C, black indicates more absorption change for horizontal than for the vertical grating stimuli. Hence the trends of increased absorption change and increased scattering change coincide. Here, in fOCT we assume there are only scattering changes. A pixel by pixel comparative t-test of the ratio calculated by Eq. (1) was done for the horizontal against the vertical grating stimuli. The tests revealed that the results obtained were statistically significant to within a 5% tolerance limit.

From the fOCT map shown, we can infer the following facts: (1) There is a discrete distribution of activation patches across depth and is stimulus specific. (2) In the very superficial region of less than 100–200 μm, there are no activation patches indicating this superficial region may correspond to layer 1 where neurons are scarce. (3) In the regions deeper than 100–200 μm, there exist several localized patches across depth showing no regular structure. (4) The localized patches extend up to the measured depth of around 1 mm.

To address whether the signals represent the regional difference of neural activity, we compared the intensity variation across the scanned line on the surface of OISI map with the integrated profile of fOCT. The integrated profile was calculated by inte-

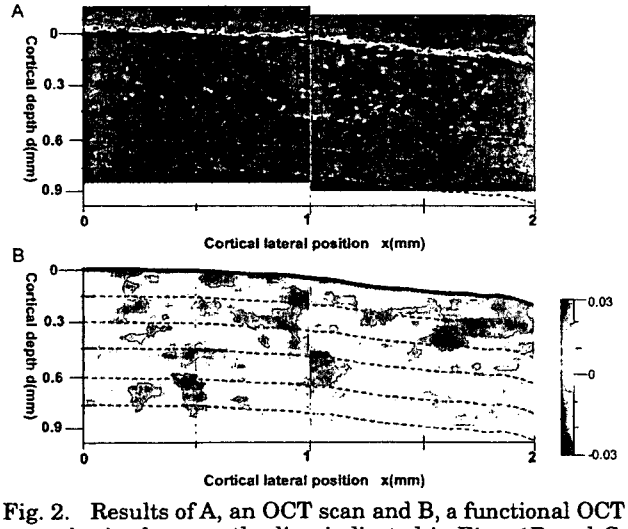

Fig. 2. Results of A, an OCT scan and B, a functional OCT map obtained across the line indicated in Figs. 1B and C. In B, the red and blue patches, respectively, represent the activated regions for horizontal and vertical gratings.

Table 1. Correlation Coefficients Between the Profiles Obtained by the OISI and fOCT Intensity Profiles Obtained from Different Scan Positions of a Single Cat under Two Different Stimulus Conditions

Position	0° −90°	45° −135°
1	0.58	0.65
2	0.32	0.29
3	0.24	0.39
4	0.89	0.77
5	0.407	0.539
6	0.566	0.559

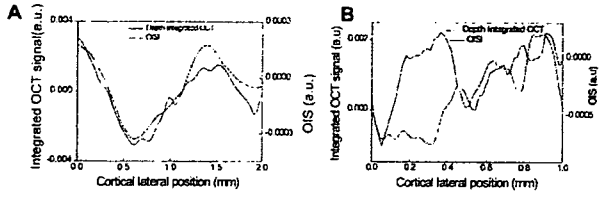

Fig. 3. Consistency of the OISI result with the integrated result of fOCT corresponding to correlation coefficients of A, 0.68 and B, 0.3. In A, the green line indicates the variation of OISI across the line indicated in Fig. 1C, and the red line is obtained by calculating the functional signal from integrating the OCT scans across the full scanned depth range of Fig. 2A. B is another example obtained from a different cat.

grating the OCT scans across the whole of the scanned depth range, followed by calculation of the differential OCT signal as described earlier in 1-D as in [6]. Here, the integration of the signal was done by summing up all the pixels across the direction of z to obtain a profile that varies across x. Figure 3A shows the result of such a comparison, with the red line indicating the integrated result and the green line indicating the OISI intensity variation across the respective lines for the example shown in Fig. 1C. A clear and remarkable agreement between the profiles could be seen corresponding to a correlation coefficient of 0.68. This indicates that the fOCT signal is indeed correlated with OISI and thus correlated with the neural-activity-evoked changes.

Experiments were done in 5 cats and found that a good correlation exists between the integrated fOCT signal and the intensity profiles obtained from intrinsic maps. Correlation coefficients vary in the range of 0.3 to 0.9. Table 1 gives the results of correlation coefficients for two different cases, namely 0°–90 ° and 45 °–135° stimuli obtained from a cat under different scan positions. Correlation coefficients vary largely across both scan positions and stimulus conditions. To make the correlation relation clear, we have also conducted a comparative study between fOCT and electrophysiology, by which the neural activity is directly measured. We found a good correlation exists between the two sets of results, which will be published elsewhere.

As an indirect way of monitoring the activity of neurons, OISI is one popular technique, and it can provide an indirect measure of the population activity. However, by its arrangement, the information obtained by the technique is integrated, and there is no way to discriminate the layer-specific information. By definition OCT could obtain structural information that is depth resolved. In this work, we have demonstrated that fOCT can become a potential tool in neuroimaging through monitoring dynamic changes in the neural system under stimulation.

References

1. T. Bonhoeffer, A. Grinvald, in *Brain Mapping–The Methods*, A. W. Toga and J. C. Mazziotta, eds. (Academic, 1996), pp. 55–97.
2. D. Y. Ts'o, R. D. Frostig, E. E. Leike, and A. Grinvald, Science **249**, 417 (1990).
3. M. Tanifuji, in *The Primate Visual System*, J. H. Kaas and C. E. Collins, eds. (CRC, 2004), pp. 345–363.
4. D. H. Hubel, *Eye, Brain and Vision* (Scientific American Library, 1995).
5. B. E. Bouma and G. J. Tearney, *Handbook Of Optical Cohrence Tomography* (Marcel Dekker, 2002).
6. R. Uma Maheswari, H. Takaoka, H. Kadono, R. Homma, and M. Tanifuji, J. Neurosci. Methods **124**, 83 (2003).
7. R. Uma Maheswari, H. Kadono, R. Homma, and M. Tanifuji, Proc. SPIE **5140**, 77 (2003).
8. M. Lazebnik, D. L. Marks, K. Potgieter, R. Gillette, and S. A. Boppart, Opt. Lett. **28**, 1218 (2003).
9. X.-C. Yao, A. Yamauchi, B. Perry, and J. S. George, Appl. Opt. **44**, 2019 (2005).
10. K. Bizheva, R. Pflug, B. Hermann, B. Povazay, H. Sattmann, P. Qiu, E. Anger, H. Reitsamer, S. Popov, J. R. Taylor, A. Unterhuber, P. Ahnelt, and W. Drexler, Proc. Natl. Acad. Sci. **103**, 5066 (2006).
11. V. J. Srinivasan, M. Wojtkowski, J. G. Fujimoto, and J. S. Duker, Opt. Lett. **31**, 2308 (2006).
12. A. D. Aguirre, Y. Chen, J. G. Fujimoto, L. Ruvinskaya, A. Devor, and D. A. Boas, Opt. Lett. **31**, 3459 (2006).
13. T. Bonhoeffer and A. Grinvald, J. Neurosci. **13**, 4157 (1993).

The effective resolution of correlation filters applied to natural scenes

Michel Vidal-Naquet Manabu Tanifuji
Riken, Brain Science Institute
Hirosawa 2-1, Wako Shi
Saitama 351-0198, Japan
michel@brain.riken.jp

Abstract

In this paper, we measure the responses of image patches, used as filters, on different image ensembles and examine how the responses are affected by reducing the resolution of the image ensembles. By comparing the set of responses obtained at high and reduced resolutions, we find that for the ensembles of natural and object images (cars), there is a limit resolution of about 15x15 and 10x10 pixels, respectively, beyond which the filter responses are significantly affected by resolution reduction. We support the result by a simple theoretical analysis based on image ensemble statistics.

There are two consequences to this result. First, it provides a natural working resolution, determined solely from the image ensemble statistics, to which higher resolution templates can be reduced without losing a significant amount of information. This can be used, in particular, to reduce the search space for useful visual features in many applications. Secondly, in contrast to many studies, it suggests that features that are more complex than Gabor patches can be effectively used as first layer filters and combined in order to represent more complex shapes and appearances.

1. Introduction

In computer image analysis, useful visual information is generally extracted from an input image by first applying a set of filters, or features, in order to simplify the image representation and facilitate further high level tasks. Success of the feature extraction step is critical for applications such as object recognition or determining correspondences in pairs of images, and depends largely on the quality of the feature selection. While many approaches use low-level descriptors based on local operations that can be computed efficiently [16, 3, 6], other popular methods consist of using a simpler representation based on feature appearance, i.e. the two-dimensional gray-level matrix. Appearance based features that were tested throughout the literature vary greatly in size and complexity, from small and generic [12, 15, 23] to intermediate complexity image fragments, often selected with an exhaustive search [8, 21, 1, 18], and full-object templates [20]. In these approaches, computation of visual similarity is performed by convolution or Normalized Cross-Correlation (NCC). Reasons for their popularity include mathematical interpretation (projection onto a feature space), invariance to contrast changes (with NCC), and also because the features can be generic as well as class-specific. The fact that correlation type operations perform rigid, pixel-wise comparisons between image patches, however, forms a critical limitation of many of these methods. Natural variation in the appearance of visual objects and scenes suggests that, on the contrary, some degree of flexibility should be incorporated into the similarity measure. Several approaches that account for local appearance variability have therefore been proposed, such as decomposing rigid features into sub-features [4, 9], using global gray-level or local gradient histograms [17, 7], and the blurring of fine details by combining a small number of feature principal components [5].

In this paper, rather than understanding how to deal with local variability in images, we attempt to uncover the visual properties of image ensembles that can be effectively captured by rigid matching of patches, using NCC as a visual similarity measure. In particular, we aim to estimate a limit of visual detail, i.e. resolution, that is determinant for the set of filter responses, measured over some image ensembles, such as the ensembles of natural images, car images, or random noise images. For this, we compute a set of responses of square *filter patches* measured on a large set of randomly selected *test patches*, represented at some high resolution, and observe the evolution of the responses as the resolution of the filter and test patches is progressively reduced. Because low frequency components dominate the spectrum in natural and car images [13, 19], the response set of patches on natural and car image ensembles is not significantly af-

fected by the low-pass filtering up to some limit resolution beyond which the set of responses is significantly affected. The evolution of the response set is measured by comparing the responses at high resolution to the responses at lower resolutions with Normalized-Cross Correlation. In addition to simulations, we perform a theoretical analysis that shows how the limit depends on the spectrum of the image ensembles and supports the quantitative results. We find that for natural images and cars, the limit resolution is of about 15x15 and 10x10 pixels, respectively.

The rest of the paper is organized as follows. In Section 2, we describe the image ensembles used in our experiments. In Section 3, we explain how we compute the patch response sets and our method to determine the effective resolution of the patches. In Section 4, we provide a theoretical analysis that explains the evolution of the filter-patch response sets as the resolution is reduced. In Section 5, we show the simulation results demonstrating the resolution limit for natural images and cars. We also provide comparisons with ensembles of random images. Finally, in Section 6, we provide a discussion of the results and a conclusion.

2. Image ensembles used and patches

In this section, we describe the different image ensembles that we tested, the extraction of the patches and explain exactly what we mean by resolution.

2.1. Images Ensembles

In our experiments, we used an ensemble of 600 natural images, taken from the commonly used database introduced in [22], and a set of 1275 car images, mostly seen from the side, appearing at scales varying by a factor of about 2, with some clutter in the background. The car images were downloaded from the internet. The natural images were of size 1024x1536, and the car images were of about 60x82 pixels. Examples of these images are shown in Figure 1.

In addition, we also tested patches from an ensemble of random images, with a predefined Fourier amplitude spectrum of the form $f^{-0.5}$, where f is the L2 norm of the 2-D frequency, in order to confirm our theoretical model (Section 4). Examples of patches, randomly selected from the different image ensembles and at different resolutions are shown in Figure 2.

2.2. Definition of resolution

We define the resolution of a patch P_s by its size s, corresponding to the Nyquist frequency after filtering with a blurring Kernel $\mathbf{G}_s$. The bold font represents the Kernel in Fourier space. The low-pass blurring Kernel used is the Hanning window, commonly used for image sub-sampling.

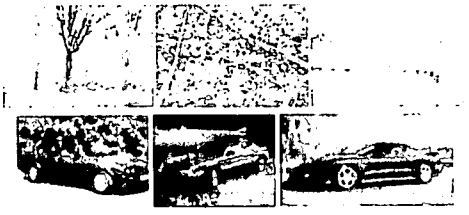

Figure 1. Examples of images from the natural and car image sets used. Natural images are log-scaled for presentation.

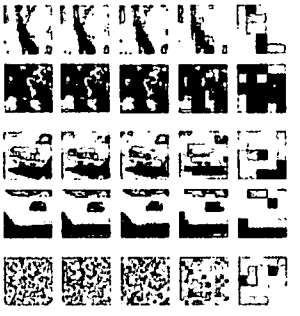

Figure 2. Examples of image patches extracted from natural scenes (top 2 lines), cars (lines 3 and 4) and random images with Fourier spectrum of the form $f^{-0.5}$ (lower line). The patches are shown at different resolutions along the horizontal axis, left to right: 41 (full resolution), 31, 21, 11 and 5 pixels per side.

The finest resolution was $s_0 = 41$, and we tested various resolution for s, down to $s = 5$.

For example, the top right patch shown in Figure 2, P_5, of size 5x5, was obtained by filtering and down-sampling P_{41}: $P_5 = \downarrow F^{-1}(\mathbf{P}_{41}.\mathbf{G}_5)$, where F^{-1} is the inverse Fourier transform and $\downarrow$ is the down-sampling operator.

3. Patch responses and Resolution Similarity Function

For a given image ensemble, we want to understand how the responses of a filter patch, extracted from the ensemble and measured on a large number of patches from the same ensemble, are affected when the resolution of the patches is reduced. We first define the Patch Response Vector and then the Resolution Similarity Function (RSF), that measures the similarity between patch responses at different resolutions.

3.1. Patch Response Vector

The set of responses of a filter patch P_s, of resolution characterized by the size s, is represented by a vector $\mathbf{V}_s$ that we call the Patch Response Vector (PRV), whose entries $V_{i,s}$ are defined by equation (1):

$$V_{i,s} = P_s \otimes T_{i,s} = \downarrow (P_{s_0} * G_s) \otimes \downarrow (T_{i,s_0} * G_s) \quad (1)$$